Performance improvement of AlN/GaN-based intersubband detectors thanks to quantum dot active regions

Daniel Hofstetter[a], Joab Di Francesco[a], Esther Baumann[b], Fabrizio R. Giorgetta[b], Prem K. Kandaswamy[c], Aparna Das[c], Sirona Valdueza-Felip[c], and Eva Monroy[c]

[a]Institute of Physics, University of Neuchâtel, 51 Avenue de Bellevaux, CH – 2000, Neuchâtel, Switzerland
[b]Optoelectronics Division, NIST, 325 Broadway, Boulder, CO 80305

[c]CEA Grenoble, INAC/SP2M/PSC, 17 rue des Martyrs, 38054 Grenoble cedex 9, France

ABSTRACT

Since the operating mode of 1.55 µm AlN/GaN-based intersubband photodetectors is based on optical rectification, both the excited state lifetime and the lateral displacement of the carriers play an important role for performance optimization. We thus show here results of an improved detector generation based on a novel type of active region. Thanks to the use of quantum dots instead of quantum wells, a factor of 60 could be gained in terms of maximum responsivity. In addition, the maximum performance was achieved at a considerably higher temperature of 160 K instead of 80 K as typically seen for quantum wells.

Keywords: Quantum dots, near-infrared, photodetectors, III-nitrides

1. INTRODUCTION

Research on mid- and near-infrared absorption via intersubband (ISB) transitions in AlN/GaN-based quantum wells (QWs) was initiated by C.F. Gmachl at Bell Laboratories in 2000 [1] and by N. Suzuki at Toshiba Corporation in Tokyo, Japan [2]. For a couple of years, absorption experiments approaching the technologically relevant wavelength range around 1.55 µm were the only progress in this domain. Starting in 2003, AlN/GaN-based photodetectors for 1.55 µm became available [3], [4], and nitride ISB technology experienced increasing attention in research. Most recent milestones in this area include the demonstration of high-frequency detection [5], the successful operation of quantum cascade detectors [6], and the discovery of optical rectification in such structures [7]. One important point, however, could not be clarified until recently: Some of the early devices showed a surprisingly high room temperature response; a feature which could not systematically be reproduced until late 2008 [8]. Temperature dependent analysis of these new structures including lateral conductivity, photoluminescence (PL), absorption, and response measurements allowed us to verify now the important role of the QW morphology. More specifically, our recent experiments reveal that the responsivity of detectors having nanostructured quantum dot (QD) like active regions offer nearly two orders of magnitude higher responsivities than their QW like counterparts. Since QWs for nitride-based near-IR devices are as thin as 5 to 6 monolayers (MLs), interface roughness can introduce significant in-plane carrier localization, which is enhanced by the polarization-induced internal electric field in these materials. Therefore, the difference between nitride-based QWs and QDs is not as well defined as in other material systems, and needs to be analyzed carefully. In this paper, we thus start with the general features of such III-nitride ISB detectors, proceed with a general characterization of QW and QD active regions, and then present a comparison between QW-based and QD-based AlN/GaN ISB photodetectors. Given the operating mechanism of such devices (nonlinear optical rectification), some QD specific design features such as coupling to the 2-dimensional wetting layer are believed to be responsible for the marked performance improvement seen in the QD samples [9].

2. OPTICAL RECTIFICATION

In contrast to most other photodetectors, GaN-based intersubband devices work in a different mode of operation, namely by optical rectification. This optically non-linear process can be understood best in a situation such as depicted in figure 1b). A step-shaped QW contains the electronic ground state in its narrow section, whereas the two excited states are located in the wider section of the well. In this configuration, an optical transition between the ground state E_1 and the first excited state E_2 is always accompanied by a lateral displacement of the electron. This becomes clear if one looks at the position of the center of gravity of the electronic wavefunctions E_1 and E_2. While E_1 is located towards the left, E_2 is "living" more on the right side of the QW. Since the donor atoms remain at their initial place, namely in the narrow part of the QW, an electrical polarization is built up for each such spatially separated electron-doping atom pair. The size of the corresponding non-linear optical coefficient $\chi_{0,\max}$ can in this situation be calculated via

$$\chi^{(2)}_{0,\max} = 2\frac{q^3 T_1 T_2}{\varepsilon_0 \hbar^2}(\rho_1 - \rho_2)\mu_{12}^2 \delta_{12} \qquad (1)$$

where q is the elementary charge, T_1 the lifetime in the excited state, T_2 the dephasing time (related to the linewidth of the transition), ρ_1-ρ_2 the difference between the sheet carrier densities in the fundamental and in the excited states, ε_0 the vacuum dielectric constant, $\hbar$ the Planck constant, μ_{12} the dipole matrix element of the transition, and δ_{12} the electron displacement. If either the lifetime or the lateral displacement of the excited electrons can be extended by some more or less sophisticated mechanism, a substantial fraction of electrons can be pumped into the upper state leading to a measurable polarization voltage under illumination. In the III-nitrides (see figure 1c)), where internal polarization fields give an asymmetrical shape to our QWs, exactly the same behavior can be observed. The only disadvantage is the fact that the size of the asymmetry is given by material parameters and cannot be determined freely. Therefore one has to find a different means to tailor the important quantities such as upper state lifetime and lateral displacement. As a side remark, it is clear that the term "lateral" in the band diagrams of figure 1 means in fact "in growth direction".

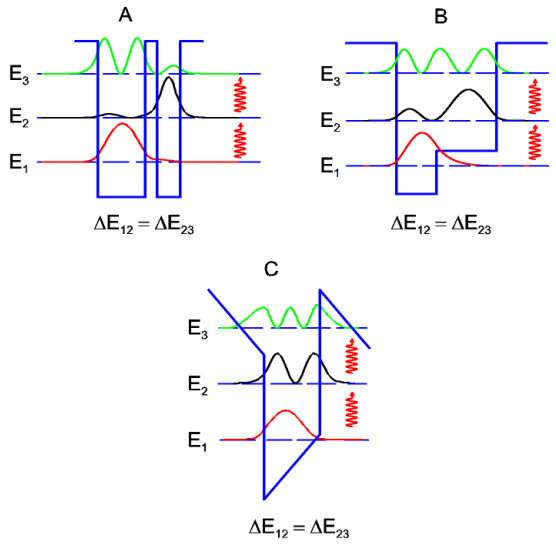

Fig. 1. Band diagrams of different configurations allowing the observation of optical rectification. 1a) presents a pair of coupled QWs, 1b) is a step QW, and 1c) shows the asymmetric situation as encountered in GaN QWs. In all three cases, the electron undergoes a lateral displacement (in growth direction) when being excited from E_1 to E_2.

The easiest way to positively influence the relevant physical parameters of the optical rectification coefficient is the use of QDs instead of QWs in the active region of these detectors. As the more detailed band diagram in figure 2 shows, QDs are always grown on a so-called wetting layer. In the III-nitride material system, this GaN wetting layer is 2 ML or 0.5 nm thick. On top of the wetting layer, dots with a height of 3 – 5 ML or a thickness of 0.75 – 1.25 nm are grown. Therefore the typical total QD dimension in growth direction can be estimated to 1.5 nm. Transmission electron

microscopy and atomic force microscopy characterization have shown that the actual lateral dot size was 4 – 6 nm. A typical TEM characterization of such QDs is shown in figure 3 below. Going back to the band diagram in figure 2, one sees that the ground state of the wetting layer (shown in yellow) can be aligned in resonance to the first excited state of the QD, namely the p_z-state (shown in red). This is a particularly important experimental situation where the electron, once excited into this p_z-state, has the possibility to scatter into the wetting layer ground state. Should the electron choose to do so, then this would lead to a larger lateral displacement (z-direction), namely roughly 1 nm instead of only 0.2 nm, but it will also result in an in-plane transfer away from the QD center (x- and y-directions). From there, returning to the electronic ground state, the s-state (blue), will take a considerably longer time, mainly due to the reduced dipole matrix element between the two ground states and to the much larger density of states in the 2-dimensional wetting layer: all places in the 1-dimensional QD ground state will be occupied already. By using QDs instead of QWs, one can therefore hope to increase both the displacement *and* the lifetime by a factor of 5 – 10 each. This should, in theory, result in a performance improvement of roughly a factor of 25 – 100.

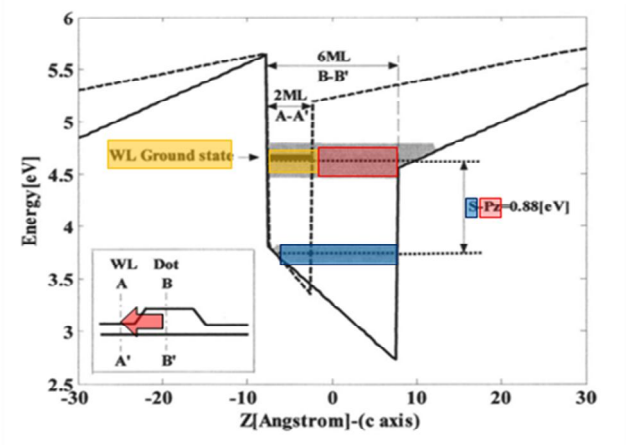

Fig. 2. Detailed band diagram of the wetting layer – quantum dot system. The ground state of the dot is shown in blue, while the ground state of the wetting layer is yellow. The latter state is shown in resonance with the excited state of the dot, shown in red.

It is clear that the experimental reality might be somewhat more subtle than explained here. For instance it is not so easy to decide from which point on a slightly rough QW can be considered as a quantum-mechanical system containing a wetting layer plus QDs. In order to have a good criterion at hand, we usually perform temperature dependent photoluminescence measurements and investigate the intensity drop when approaching room temperature. A good QD sample shows a nearly constant intensity up to 150 – 200 K, whereas a QW sample starts to drop already below 50 K. As we will see later, the overall drop between 10 K and 300 K is on the order of a factor of 3 for a QD, while being typically a factor of 50 or more for a QW.

3. FABRICATION/EXPERIMENTS

In order to make a fair comparison, we fabricated two detector devices coming from the same growth batch. Except for the active region, which was QW-based in one case and QD-based in the other, all layer thicknesses and doping levels were identical. Epitaxial growth of the detector layers was based on plasma-assisted molecular-beam epitaxy on 1 µm thick AlN-on-sapphire substrates. On top of this first AlN layer, we grew a 500 nm thick AlN buffer followed by a 40 period active region, and a 100 nm thick AlN cap layer. The active region was either a superlattice consisting of 1.5 nm thick *n*-doped ([Si] = 2×10^{19} cm^{-3}) GaN QWs separated by 5 nm thick undoped AlN barrier layers, or a superlattice with GaN QDs resulting from N-rich deposition of 4 ML of *n*-doped ([Si] = 2×10^{19} cm^{-3}) GaN and being separated by 5 nm thick undoped AlN barriers. For the growth conditions used for such QD samples, TEM characterization revealed indeed a wetting layer thickness of roughly 2 ML, a QD height on the order of 1 nm, and a lateral dot size of about 4 – 6 nm [10]. The density of these truncated hexagonal dots was 1 – 2 x 10^{12} cm^{-2} resulting in an electron density of 2 electrons per dot. In contrast, typical QW samples have smooth layers with an interfacial roughness at the monolayer scale [11].

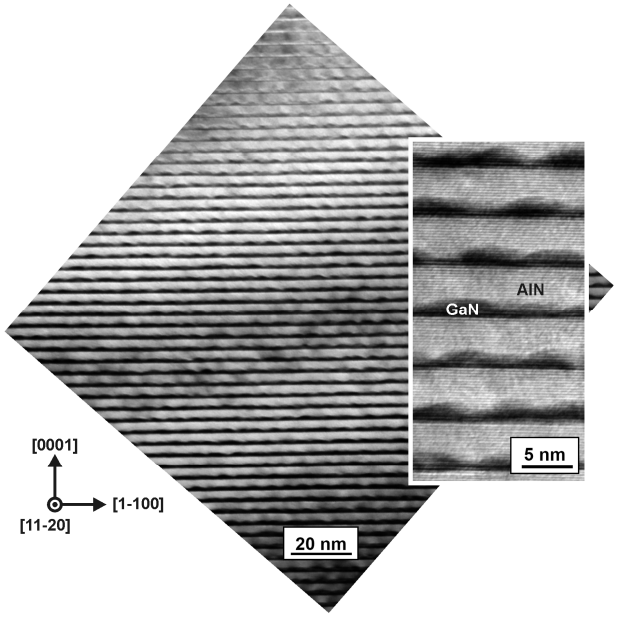

Fig. 3. Transmission electron spectroscopy image of a QD superlattice. The images show that the wetting layer has a thickness of 2 monolayers (0.5 nm), and that the dots are 4 – 6 nm wide and 1.5 nm thick.

Figure 4 shows an Arrhenius plot of the differential resistance around 0 V and measured in lateral direction along the QW/QD layers. For temperatures between 200 K and 300 K, the QW differential resistance presents a thermal activation energy of E_a^{QW} = 16.4 meV, while the QD curve shows a considerably higher value of E_a^{QD} = 73.8 meV. The simulated band structure of one active region period of the QD sample is shown in the inset of figure 4. Bound-to-bound transition energies of 780 meV and a dipole matrix element of 3.5 Å are predicted [12]. Since the probability of resonant tunneling across 5 nm thick AlN barriers is very small, *no electron transport through the barriers* takes place. Again it is well visible that the lateral displacement into the wetting layer ground state δ_{13} is much larger than the one into the QD first excited state δ_{12} [6].

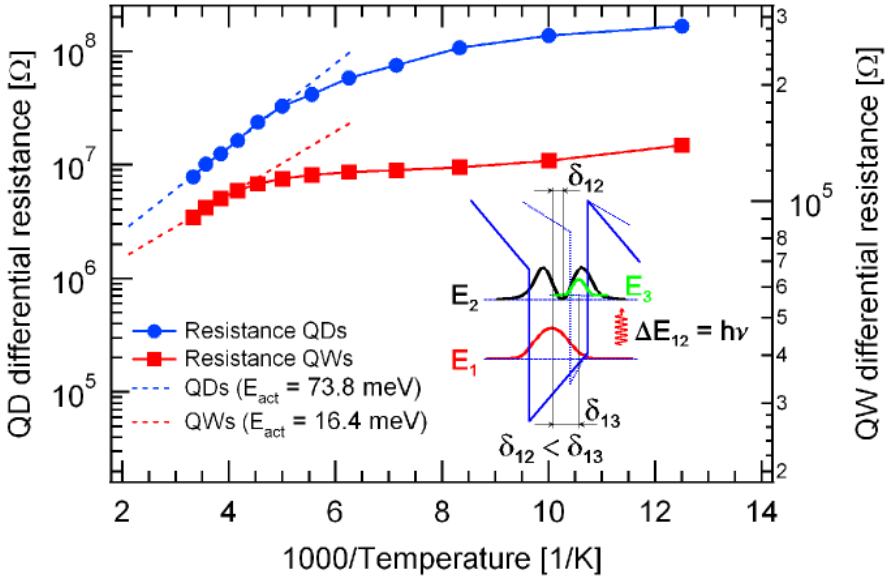

Fig. 4. Arrhenius plots of the differential resistance values around 0 V. By taking into account temperatures >200 K only, activation energies of 16.4 meV and 73.8 meV were found for the QW and the QD samples respectively. The inset shows a simulated band structure of the QD sample with three relevant electronic states.

After growth, the samples were prepared as multi-pass zigzag waveguides (3.2 mm long for the QWs, 2.0 mm long for the QDs) with a polished back and two parallel polished faces at angles of 45° to the surface normal. This configuration allows efficient coupling of the incoming light into the waveguide, enables a good interaction between the ISB transition and the radiation, and offers equal Fresnel losses for both TE and TM polarization. Thermal evaporation of stripe-shaped Ti/Au (10/400 nm) contacts running perpendicularly to the 45 ° facet mirrors and having a width of 0.8 mm completed device processing. The finished samples were then glued on copper heatsinks and wire bonded for electrical characterization. A schematic overview of the experimental setup is shown in figure 5. During the measurements, the detectors were placed in a liquid nitrogen-flow cryostat. Illumination was done using the internal white light source of a Fourier transform infrared (FTIR) spectrometer (Bruker AFS-66), while the produced detector signals were amplified with an EG&G Instruments (Model 5113) voltage pre-amplifier and fed back into the external detector port of the FTIR.

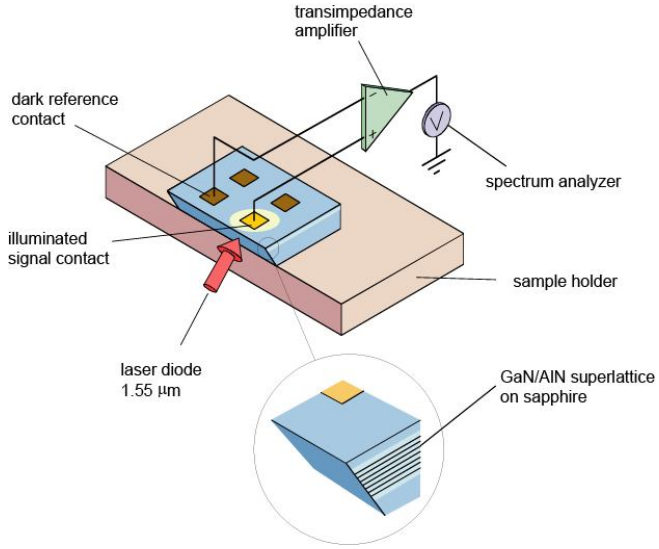

Fig. 5. Experimental preparation for the two samples showing the simple fabrication procedure based on electrical contact evaporation and wedge polishing. The electrical signals can be detected between the illuminated signal contact and the dark reference contact.

In order to further assess the different carrier confinement in the samples, temperature dependent continuous wave PL experiments using a frequency-doubled Argon laser emitting at 244 nm were performed. Figure 6 shows the logarithmic signal intensity vs. inverse temperature. While the QW sample has a constant intensity up to 30 K only, the QD sample's PL is nearly constant up to temperatures on the order of 160 K. The improved thermal stability of the QD PL signal is due to three-dimensional carrier localization in the dots, which hinders the electrons from moving towards non-radiative recombination centers [13]. In order to quantify the energetic barrier that the electrons need to surmount to reach the non-radiative recombination centers, we can apply the following equation [14]

$$I(T) = I_0 / \left[\left(1 + a_1 \exp \frac{-E_{a1}}{kT} \right) \left(1 + a_2 \exp \frac{-E_{a2}}{kT} \right) \right] \qquad (2)$$

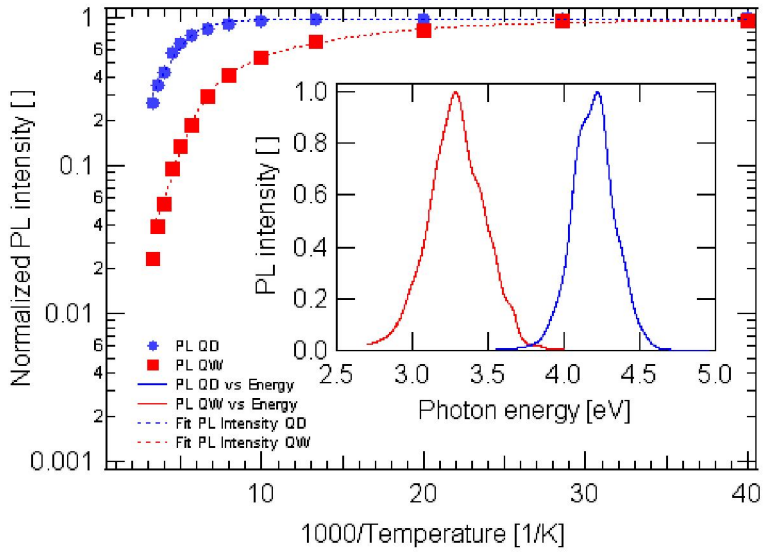

Fig. 6. Thermal evolution of the PL intensity of typical QW and QD samples. Solid lines are fits to eq. 2, yielding activation energies of 17 meV and 102 meV for the QWs and about 79 meV for the QDs. The inset shows normalized PL spectra at 7 K for both samples.

where $I(T)$ is the PL intensity as a function of temperature, I_0 the PL intensity at 0 K, E_{a1} and E_{a2} are the activation energies involved in the carrier escape, a_1 and a_2 are fitting constants, and k is Boltzmann constant. This general equation assumes two non-radiative recombination paths that are related, the electron confinement being estimated from the lower activation energy. Figure 6 presents the fit of the thermal evolution of the PL intensity of QWs and QDs to eq. 2. Thermal activation energies of 17±2 meV and 79±5 meV were extracted for the QWs and QDs, respectively. These values are in good agreement to the ones found from the above-described transport measurements. The inset of figure 6 shows a comparison between the PL spectra of QWs and QDs. Taking into account the nearly 100 % occupation of the QD ground state, we propose that the QD ISB transition energy (0.87 eV) plus the QW IB energy (3.3 eV) should equal the QD interband energy (4.2 eV). Since the experimental findings in figures 6 and 7 confirm this very well, the effective QD plus wetting layer "thickness" must be exactly equal to the one of the QW thickness.

4. RESULTS

Multi-pass (8 and 5 passes through QW and QD, respectively) TM-polarized absorption curves as a function of temperature measured from 100 K to 300 K are shown in Fig. 7 (left) for the QW sample and Fig. 7 (right) for the QD sample. The absorption lines are attributed to transition between the two first electron confined states in the QWs (e_1-e_2) and to transition from the s ground level of the QD to the first excited level along the growth axis, p_z. Employing the ISB absorption formula based on Fermi's golden rule, we were able to confirm that the observed absorption peak strengths of 12% for the QDs and 19% for the QWs along with the full widths at half maximum (FWHM) cited below corresponded indeed to relatively low doping levels on the order of 1.6×10^{19} cm^{-3} for the QWs and 2.5×10^{19} cm^{-3} for the QDs. It is also interesting to note that the absorption of the QDs shows a clean single peak, whereas the one from the QWs contains some modulation, similar as observed by other authors [15]. In contrast to earlier interpretations such as ML fluctuations, we attribute this effect to coupling of the QW excited state with multiple conduction band ground states occurring due to Brillouin zone folding. The peak absorption lies at 7220 cm^{-1} (1.39 µm, 895 meV) for the QD (FWHM = 760 cm^{-1}, 94 meV) and 6560 cm^{-1} (1.52 µm, 813 meV) for the QW sample (FWHM = 1150 cm^{-1}, 142 meV). These numbers confirm our prediction from PL and correspond to literature values for the QW and QD dimensions used in these experiments. We observe neither temperature induced broadening nor strong absorbance changes in the two samples.

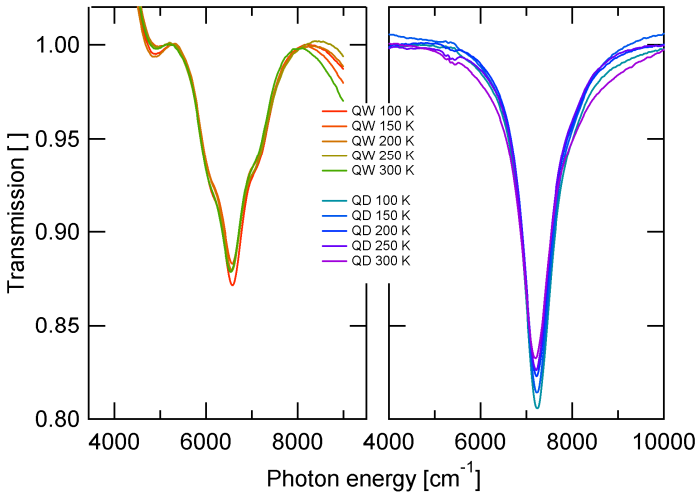

Fig. 7. Comparison between the transmission spectra of the quantum well (left) and the quantum dot (right) samples. The transmission spectra are recorded as a function of temperature (100, 150, 200, 250, and 300 K). A minimal broadening effect along with slight reduction can be observed.

Finally, we present in Fig. 8 the spectral response of both types of detectors. The spectral peak position and FWHM of the QW response are 6700 cm^{-1} (1.49 µm, 830 meV) and 1500 cm^{-1} (185 meV), respectively. In contrast, the QD sample peaks at 7000 cm^{-1} (870 meV, 1.43 µm) with a FWHM of 1800 cm^{-1} (223 meV). The inset of figure 8 shows normalized peak response vs. temperature curves for both QW and QD detectors. For the QWs, the maximum response of 0.17 V/W is reached at 80 K, and the signal drops by more than one order of magnitude from 80 K to room temperature. In contrast, the QD sample reaches its maximum responsivity of 10 V/W at a considerably higher temperature, namely at 160 K. According to equation 1 [6], this performance improvement can be explained by both a longer carrier lifetime in the excited quantum state and a larger lateral electron displacement, δ_{13}. As reported by Mukai et al. for the InGaAs/GaAs material system, the absence of electron phonon scattering can lead to carrier lifetimes on the order of 10 - 100 ps instead of only 1 ps [16]. Therefore, a certain effect of the phonon bottleneck, especially at low temperatures, cannot be ruled out. Most importantly, however, the higher density of states in the 2-dimensional wetting layer compared to the 1-dimensional QDs is the dominant factor for the slower carrier decay. Finally, strong coupling between the ground state of the QD wetting layer and the resonantly aligned p_z state could also contribute to both a longer carrier lifetime (reduced overlap) and larger electron displacement in the QDs.

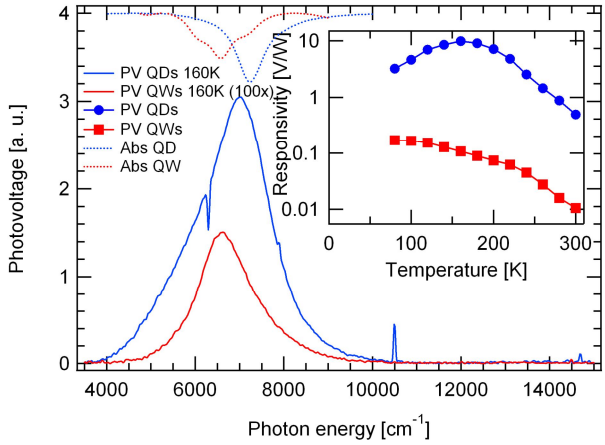

Fig. 8. Comparison between the spectral response and absorption curves (in a.u.) of the QD sample and the QW sample (100x) at 160 K. The responsivity spectra of the QD sample had to be corrected according to the formula $R_{cor} = R_{meas}$ x $\{(R_{diff} + Z_{in}) / Z_{in}\}$, where Z_{in} = 100 MΩ is the input impedance of the amplifier, R_{diff} the differential resistance of the device, R_{meas} the measured, and R_{cor} the corrected responsivity. The inset shows the corrected peak responses of QWs (red) and QDs (blue) as a function of temperature.

5. CONCLUSIONS

In conclusion, we have presented a detailed study on nitride-based QW/QD samples used for photovoltaic ISB photodetection at 1.55 μm. Both lateral conduction and PL measurements confirmed that we have indeed fabricated two different samples having either QWs or QDs in the active region. Various effects such as the larger density of states in the wetting layer, stronger localization of electrons in QDs, and coupling to the ground level of the wetting layer result in a considerably higher maximum responsivity of the QDs with respect to the QWs. Although the somewhat longer carrier lifetime might have a slightly detrimental effect on the overall detector speed, 100 GHz operation is still a realistic goal for such devices.

REFERENCES

[1] C. Gmachl, H.M. Ng, S.N.G. Chu, and A.Y. Cho, "Intersubband absorption at λ= 1.55 μm in well- and modulation-doped GaN/AlGaN multiple quantum wells with superlattice barriers," Appl. Phys. Lett., vol. 77, pp. 3722-3724, 2000.

[2] N. Suzuki and N. Iizuka, "Effect of polarization field on intersubband transition in AlGaN/GaN quantum wells," Jap. J. Appl. Phys., vol. 38, pp. L363-L365, 1999.

[3] D. Hofstetter, S.-S. Schad, H. Wu, W.J. Schaff, and L.F. Eastman, "GaN/AlN-based quantum well infrared photodetector for 1.55 μm," Appl. Phys. Lett., vol. 83, pp. 572-574, 2003.

[4] D. Hofstetter, E. Baumann, F.R. Giorgetta, M. Graf, M. Maier, F. Guillot, E. Bellet-Amalric, E. Monroy, "High-quality AlN/GaN-superlattice structures for the fabrication of narrow-band 1.4 μm photovoltaic intersubband detectors," Appl. Phys. Lett., vol. 88, no. 121112, 2006.

[5] F.R. Giorgetta, E. Baumann, F. Guillot, E. Monroy, and D. Hofstetter, "High frequency (f=2.37 GHz) room temperature operation of 1.55 μm AlN/GaN-based intersubband detector," Electron. Lett., vol. 43, pp. 185-187, 2007.

[6] A. Vardi, N. Kheirodin, L. Nevou, H. Machhadani, L. Vivien, P. Crozat, M. Tchernycheva, R. Colombelli, F.H. Julien, F. Guillot, C. Bougerol, E. Monroy, S. Schacham, and G. Bahir, "High-speed operation of GaN/AlGaN quantum cascade detectors at λ = 1.55 μm," Appl. Phys. Lett., vol. 93, no. 193509, 2008.

[7] D. Hofstetter, E. Baumann, F.R. Giorgetta, F. Guillot, S. Leconte, and E. Monroy, "Optically nonlinear effects in intersubband transitions of GaN/AlN-based superlattice structures," Appl. Phys. Lett., vol. 91, no. 131115, 2007.

[8] D. Hofstetter, E. Baumann, F.R. Giorgetta, R. Théron, H. Wu, W.J. Schaff, J. Dawlaty, P.A. George, L.F. Eastman, F. Rana, Prem K. Kandaswamy, S. Leconte, and E. Monroy, "Photodetectors based on intersubband transitions using III-nitride superlattice structures," Journal of Physics: Condensed Matter, vol. 21, no. 174208, 2009.

[9] H. Frohlich and T.K. Mitra, "Superconductivity in metals with incomplete inner shells," Journal of Physics C: Solid State Physics, vol. 1, pp. 544-548, 1968.

[10] F. Guillot, E. Bellet-Amalric, E. Monroy, M. Tchernycheva, L. Nevou, L. Doyennette, F. H. Julien, Le Si Dang, T. Remmele, M. Albrecht, T. Shibata, and M. Tanaka, "Si-doped GaN/AlN quantum dot superlattices for optoelectronics at telecommunication wavelengths," J. Appl. Phys., vol. 100, no. 044326, 2006.

[11] P. K. Kandaswamy, F. Guillot, E. Bellet-Amalric, E. Monroy, L. Nevou, M. Tchernycheva, A. Michon, F. H. Julien, E. Baumann, F. R. Giorgetta, D. Hofstetter, T. Remmele, M. Albrecht, S. Birner, and Le Si Dang, "GaN/AlN short-period superlattices for intersubband optoelectronics: A systematic study of their epitaxial growth, design, and performance," J. Appl. Phys., vol. 104, no. 093501, 2008.

[12] M. Tchernycheva, L. Nevou, L. Doyennette, F.H. Julien, and E. Warde, "Systematic experimental and theoretical investigation of intersubband absorption in GaN/AlN quantum wells," Phys. Rev. B, vol. 73, no. 125347, 2006.

[13] J. Renard, P.K. Kandaswamy, E. Monroy, and J. Gayral, "Suppression of nonradiative processes in long-lived polar GaN/AlN quantum dots," Appl. Phys. Lett., vol. 95, no. 131903, 2009.

[14] M. Leroux, N. Grandjean, B. Beaumont, G. Nataf, F. Semond, J. Massies, and P. Gibart, "Temperature-quenching of photoluminescence intensities in undoped and doped GaN," J. Appl. Phys., vol. 86, pp. 3721-3728, 1999.

[15] E. Baumann, F.R. Giorgetta, D. Hofstetter, H. Wu, W.J. Schaff, L.F. Eastman, and L. Kirste, "Tunnelling effects and intersubband absorption in AlN/GaN superlattices," Appl. Phys Lett. Vol. 86, no. 032110, 2005.

[16] K. Mukai, N. Ohtsuka, H. Shoij, and M. Sugawara, "Emission from discrete levels in self-formed InGaAs/GaAs quantum dots by electric carrier injection: Influence of phonon bottleneck," Appl. Phys. Lett., vol. 68, pp. 3013-3015, 1996.